NANO LETTERS

pubs.acs.org/NanoLett

Letter

Strain Engineering of Ion-Coordinated Nanochannels in Nanocellulose

JiaHao Li,[§] YuanZhen Hou,[§] ZeZhou He, HengAn Wu, and YinBo Zhu*

Cite This: *Nano Lett.* 2024, 24, 6262−6268

Read Online

ACCESS | Metrics & More | Article Recommendations | Supporting Information

ABSTRACT: Expanding the interlayer spacing plays a significant role in improving the conductivity of a cellulose-based conductor. However, it remains a challenge to regulate the cellulose nanochannel expanded by ion coordination. Herein, starting from multiscale mechanics, we proposed a strain engineering method to regulate the interlayer spacing of the cellulose nanochannels. First-principles calculations were conducted to select the most suitable ions for coordination. Large-scale molecular dynamics simulations were performed to reveal the mechanism of interlayer spacing expansion by the ion cross-linking. Combining the shear-lag model, we established the relationship between interfacial cross-link density and interlayer spacing of an ion-coordinated cellulose nanochannel. Consequently, fast ion transport and current regulation were realized via the strain engineering of nanochannels, which provides a promising strategy for the current regulation of a cellulose-based conductor.

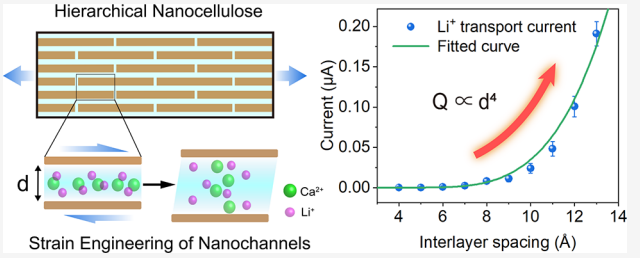

KEYWORDS: *nanocellulose, cellulose nanochannel, ion transport, strain engineering, ion cross-linking*

Solid-state lithium−metal batteries with high energy density and fast charging have been demonstrated as promising energy-storage devices used in everyday phones and electric vehicles.[1] However, manufacturing and recycling of lithium−metal anodes cause many problems such as shortage of critical metals (e.g., lithium, cobalt, and nickel),[2−4] carbon dioxide release, and soil pollution,[5−8] which poses a huge adjustment to sustainable development. To solve this problem, organic materials are used in the manufacture of electrodes because of their low cost, environmental friendliness, sustainability, and ease of recycling. As expected, the easy access in quantity from biomass and renewable nature make cellulose a quite suitable raw material for organic electrodes.[9−11] Recently, high-conductivity stable cellulose-based conductors have been achieved based on copper-ion-coordinated molecular channel engineering. They have significantly higher conductivity and reliability compared to conventional organic electrode materials and have great prospects in electrochemical synaptic devices, solid-state sensors, and redox-controlled information processing and storage.[12,13]

In nature, the plant cell wall has a tracheid structure in which cellulose nanofibrils (CNFs) are aligned along the axis to form the nanochannels and allow plants to transport water and nutrients from the soil.[14−18] Inspired by this process, nanochannels play an important role in the electrical properties of cellulose-based conductors because the interlayer spacing of nanochannels determines the conductivity of cellulose-based conductors directly. To improve the conductivity, a lot of effort has been made to engineer the interlayer spacing by ion coordination. Yang et al. verified that when cellulose is coordinated with copper ions, the interlayer spacing is expanded from 3.9 to 8.7 Å. As a result, the conductivity is highly improved from 10^{-5} to 10^{-3} S/cm, and the stability of the cellulose-based conductor is also improved.[12] Recent works showed that compared with copper ions and sodium ions, calcium-ion-coordinated cellulose-based conductors have a larger conductivity (204×10^{-3} S/cm) and higher Seebeck coefficient (27 mV/K^{-1}),[13] which implies that calcium ions may be more suitable as cross-links for the cellulose-based conductor. Experimental achievements have demonstrated the expansion of interlayer spacing through ion coordination, but there still remains a need to elucidate the underlying mechanism to effectively regulate cellulose nanochannels. Lately, the mechanism of expanding the interlayer spacing of cellulose nanochannels with ion coordination has been investigated theoretically and experimentally. The ab initio molecular dynamics simulations performed by Dong et al. showed that cellulose coordinated by copper ions forms a supramolecular framework and provides a nanochannel with ∼10 Å interlayer spacing for fast sodium ion transport.[19] They also experimentally demonstrated the structural stability of this copper-coordinated supramolecular framework in a highly

Received: February 19, 2024
Revised: May 9, 2024
Accepted: May 10, 2024
Published: May 14, 2024

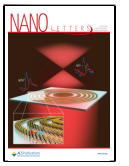

https://doi.org/10.1021/acs.nanolett.4c00867
Nano Lett. 2024, 24, 6262−6268

alkaline environment. Although ion coordination is widely used to engineer the interlayer spacing of cellulose nanochannels and improve the conductivity, it is still unclear how to regulate the conductivity by the mechanical method and what the molecular mechanisms behind the change of nanochannels are.

Strain engineering has been commonly used to regulate the interlayer spacing of many kinds of two-dimensional materials such as graphene, MoS_2, and hBN,[20−27] which have staggered structures similar to those of cellulose-based conductors.[21,28−31] In what follows, combining density functional theory (DFT) calculations and molecular dynamics (MD) simulations, we investigated the ion coordination of cellulose nanochannels and the regulation of interlayer spacing by strain engineering, which is an effective method for interlayer spacing regulation at the molecular level.[21] Cellulose can be derived from wood (Figure 1), and ions are coordinated with −OH

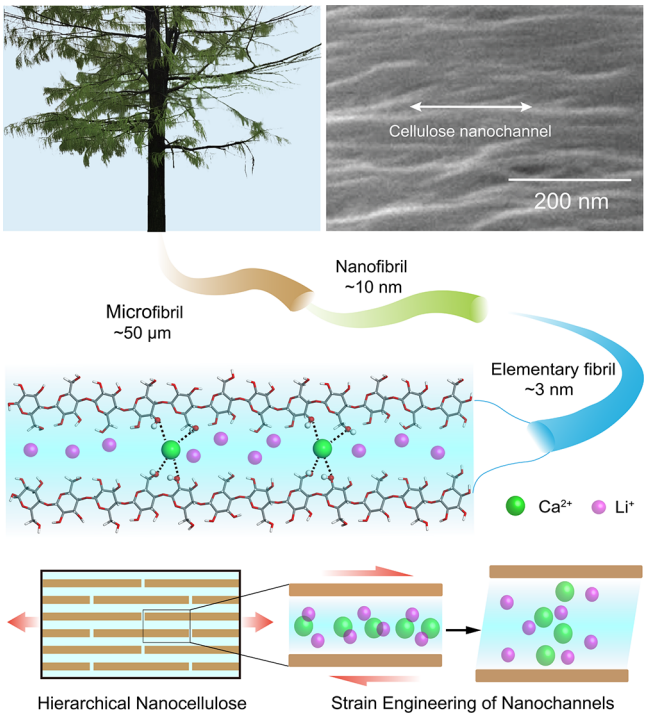

Figure 1. Schematic diagram of CNC-based hierarchical structure and the interlayer space expanding by ion coordination cross-linking and strain engineering. The expanding of channel spacing during the tensile process should provide a promising strategy for the design of cellulose-based conductors. The SEM image is extracted from ref 12. Copyright 2021 Springer Nature.

groups at the cellulose nanocrystal (CNC) interface and can expand the interlayer spacing. The cellulose-based conductors are composed of several CNFs with a length of hundreds of nanometers and have a staggered microstructure. The representative volume element (RVE) was used to represent the minimum periodic repetition unit of microstructures to withstand shear deformation during tensile process of a cellulose-based conductor (Figure 1).[32] The strain engineering and size effect of RVE were discussed in detail with the shear-lag model. Last, MD simulations were carried out to verify the influence of interlayer spacing on current of the lithium ion transport on a nanoscale. Our simulations provided molecular insight into the conductivity regulation of ion-coordinated cellulose-based conductors, which should be significant for achieving high-performance cellulose-based conductors through mechanical methods.

The key to normally ion-coordinated nanocellulose serving as ion conductors is to form stable molecular channels for fast ion transport.[33,34] Recent studies reported that metal cations can coordinate with CNFs due to the abundant of −OH groups on the molecular chains.[12] The intercalated ionic cross-links (e.g., Cu^{2+}) between CNFs can provide the steric hindrance to open the nanocapillaries for Li^+ ions. To find more suitable ionic cross-links for nanocellulose, we performed first-principles calculations to distinguish the interactions between nanocellulose and different ionic cross-links, with the model being shown in Figure S1a. Here, the coordinate bond length, interlayer spacing (Δh), and binding energy are the three main factors considered in the comparison of DFT results. Figure 2a plots Δh versus bond length for the water

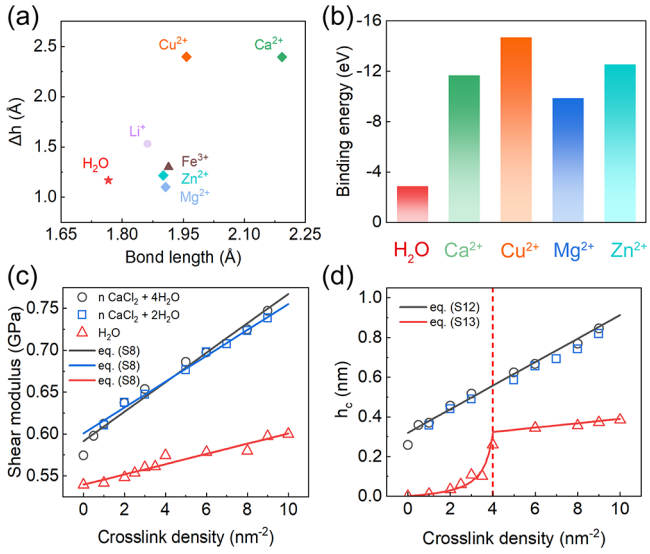

Figure 2. Interactions between nanocellulose and different intercalated media (metal cations and water molecules). (a) Channel spacing (Δh) and coordinate bond length computed from DFT calculations for different cations and water molecules intercalated between two cellulose molecular chains. (b) Binding energy comparisons of water molecules and different divalent cations (Ca^{2+}, Cu^{2+}, Mg^{2+}, and Zn^{2+}) intercalated in nanocellulose. Since Ca^{2+} exhibits the largest coordinate bond length with nanocellulose, we then chose Ca^{2+} as the representative divalent cation in the MD simulations of ion nanochannels. (c) Shear modulus as a function of cross-link density. The solid lines are fitted by eq S8. (d) RVE thickness (h_c) as a function of cross-link density. The dashed red line marks the critical point of cross-link density of water molecules intercalated in nanocellulose. The solid lines are fitted by eqs S12 and S13.

molecule and different ions intercalated between two cellulose molecular chains. It is found that Cu^{2+} and Ca^{2+} intercalated into nanocellulose exhibit the highest Δh (~2.4 Å), while their coordinate bond lengths are different (1.95 and 2.19 Å, respectively). As shown in Figure 2b, the binding energy of Ca^{2+} intercalated into nanocellulose is on the same level as that of Cu^{2+} and other divalent ions. As shown in Figure S4, the interlayer spacing is determined by the intrinsic bond length of ionic cross-linking and the attraction-force-induced bond compression between cellulose chains. On one hand, the larger intrinsic cross-linking bond lengths of Ca^{2+} and Cu^{2+} can provide more steric hindrance than other ions; on the other

https://doi.org/10.1021/acs.nanolett.4c00867
Nano Lett. 2024, 24, 6262−6268

hand, the cross-linking bonds of Ca^{2+} and Cu^{2+} are more difficult to compress by the attraction force between cellulose chains due to the higher bonding stability as measured by the binding energy in Figure 2b. In cellulose nanochannels, ions coordinate not only with the −OH groups in cellulose but also with the water molecules. The interactions among ions, water molecules, and nanocellulose interfaces significantly contribute to the interlayer spacing of cellulose nanochannels. Bond lengths of Ca^{2+} and Cu^{2+} ions coordinated with water molecules and nanocellulose are shown in Figure S1b. The DFT results show that whether it is water or cellulose, Ca^{2+} has a larger bond length than Cu^{2+}. Thus, Ca^{2+} should be a more suitable candidate of ionic cross-links in nanocellulose to form stable and wide nanochannels for fast ion transport. In the next section, our simulations and discussion focus mainly on the Ca^{2+}-intercalated cellulose nanochannels.

To evaluate the Ca^{2+}-intercalated nanochannels in nanocellulose, we performed large-scale MD simulations considering the aqueous environment and different cross-link densities. The simulation model is plotted in Figure S2. The shear modulus of the simulation model can reflect the interlayer cross-linking ability of different media intercalated into nanocellulose. As shown in Figure 2c, there is a positive proportional relationship between the shear modulus and cross-link density, which implies the mechanical properties of cellulose-based conductors can be improved by ion cross-links[35] and the relationship can be well fitted by a linear equation.[36,37] The interlayer cross-linking can be enhanced significantly with the increase of Ca^{2+} cross-link density, while the contribution of water molecules is inappreciable. It can be deduced that the interlayer cross-linking mainly relies on the cross-link density of Ca^{2+} ions. In our simulations, we found that the Ca^{2+} cross-link density can change the width of nanochannel,s which is much different from previous studies that assumed the nanochannel width (or thickness of RVE) to be a constant under different cross-link densities.[28,37,38] Here, h_c is defined as the distance between the center of mass of the upper and lower layers of the RVE. Figure 2d implies that the relationships of h_c versus cross-link density are completely distinct for Ca^{2+} ions and water molecules. For Ca^{2+} ionic cross-linking, there is also a positive proportional relationship between h_c and cross-link density, which should originate from the interlayer cross-linking ability of Ca^{2+} ions between cellulose molecular chains. However, the nanochannel width in nanocelluloses regulated by water molecules is very limited. When the cross-link density of water molecules is larger than the critical value (4 nm^{-2}), the change of h_c is negligible.

The mechanism of the critical value is explained in detail in Figure S4. The swelling of nanocellulose is not considered in our study, since the number density of water molecules is small in both experiments and our simulations.[12] Thus, wider nanochannels in nanocellulose can be achieved with an increase in the number density of Ca^{2+} ions. It should be noted that excessive cross-link density is disadvantageous. On one hand, the increasing interlayer spacing will weaken the densified arrangement of CNCs and induce more defects on interfaces, thus reducing the mechanical strength of nanocellulose materials; on the other hand, the larger interlayer spacing under higher cross-link density will significantly inhibit the efficiency of ionic transport in nanochannels. By setting the maximum interlayer spacing as 2 nm, we can predict that the upper limit of the cross-link density is 28.317 nm^{-2} using eq S14. Therefore, the moderate cross-linking density is conducive to fully exerting the mechanical properties and ion transport capacity of ionic conductors in practical applications.

Recent experiments demonstrated that mechanical pressing can change the conductivity of cellulose-derived supramolecular frameworks,[12,19] indicating that the nanochannels in nanocellulose can be engineered via a mechanical deformation. When the interlayer spacing was expanded from 3.9 to 8.4 Å,[12] the measured conductivity of a cellulose-based conductor increases almost a hundred times. The strain engineering of nanochannels had also been reported in two-dimensional (2D) materials and nanodevices, which is an important approach to achieve better performances through regulating the interlayer spacing at the molecular scale. Next, we revealed the effect of strain engineering of cellulose nanochannels. Our simulations illustrated that Ca^{2+} ions can further enlarge the nanochannels in nanocellulose when shear strain is applied. As shown in Figure 3a, it is found that the

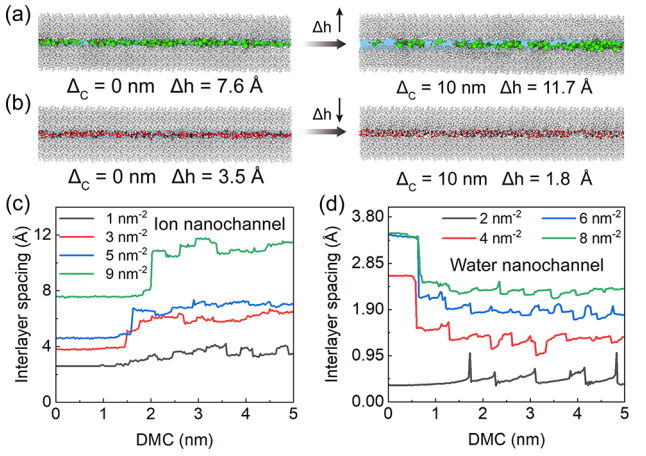

Figure 3. Strain engineering of cellulose nanochannels under shear. (a) Snapshots highlighting the increase of ion-coordinated nanochannels after shear. (b) Snapshots highlighting the reduction of water-mediated nanochannels after shear. In (a) and (b), atoms in CNCs are colored in gray, and Ca^{2+} ions and water molecules are colored in green and red, respectively. (c, d) Channel spacing as a function of the shear displacement for cases of ion-coordinated (c) and water-mediated (d) nanochannels, respectively.

increase in Δh should contribute mainly to the aggregate behavior of hydrated Ca^{2+} ions in the nanochannel. In general, the electrostatic interactions between Ca^{2+} and water molecules are stronger than the hydrogen bonds among water molecules, thus inducing significant Ca^{2+} aggregation through the bridging effects of water molecules during the shear disturbance process. While as shown in Figure 3b the cellulose nanochannel cross-linked by water molecules exhibits a diverse tendency, since water molecules are captured by the −OH groups on the (010) surface of nanocellulose. Here, Δ_C is defined as the displacement of mass center (DMC) of the upper CNC in RVE. When the DMC is 10 nm, as shown in Figure 3a–d, Δh of cellulose nanochannels cross-linked by Ca^{2+} ions increases from 7.6 to 11.7 Å, and that in the cases of water molecules decreases from 3.5 to 1.8 Å. To verify the dependence of cross-link density on the interlayer spacing of nanochannels in nanocellulose, large-scale MD simulations were carried out considering different cross-link densities of Ca^{2+} ions and water molecules. Figure 3c indicates that a higher cross-link density of Ca^{2+} ions can result in more

https://doi.org/10.1021/acs.nanolett.4c00867
Nano Lett. 2024, 24, 6262−6268

effective expansion of cellulose nanochannels. As expected, as shown in Figure 3d, the interlayer spacing of the cellulose nanochannel is suppressed by the high number density of intercalated water molecules.

To obtain a thorough understanding of the effect of interlayer spacing on different ion transports, we then collected simulation data to plot the diagram of the strain engineering of Ca^{2+}-intercalated cellulose nanochannels. As demonstrated in Figure 4, the phase diagram in the plane of cross-link density versus interlayer spacing can guide us to design nanochannels in cellulose-based conductors. Here, Ca^{2+} ions are used for the interlayer intercalation to open up the cellulose nanochannel. Under a specific cross-link density of Ca^{2+} ions, the interlayer spacing of cellulose nanochannels before and after strain engineering can be measured in MD simulations. The fitting in Figure S5 indicates that there is an approximate linear relationship between the interlayer spacing and cross-link density. The red and blue lines in Figure 4 give the upper and lower limits of interlayer spacing of Ca^{2+}-intercalated cellulose nanochannels regulated by strain engineering, respectively. In previous experiments, monovalent ions such as Na^+ and Li^+ are usually used as conducting mediums in cellulose-based conductors. While the ability of ion transport in nanochannels depends on the hydration radius of corresponding ion,[39] instead of the radius of ion itself. For example, for the same Cu^{2+}-coordinated cellulose nanochannels, Na^+ exhibits a larger conductivity than Li^+ due to the smaller hydration radius of Na^+. Under the nanoconfinements, the nanochannels with a slightly larger width will enhance the ion transport and increase the conductivity. In recent experiments, a cellulose conductor can achieve superior Li^+ ionic conductivity when the Cu^{2+}-intercalated nanochannels expand from 3.9 to8.7 Å.[12] Thus, strain engineering of nanochannels can help to regulate the ion transport and related conductivity by improving the interlayer spacing.

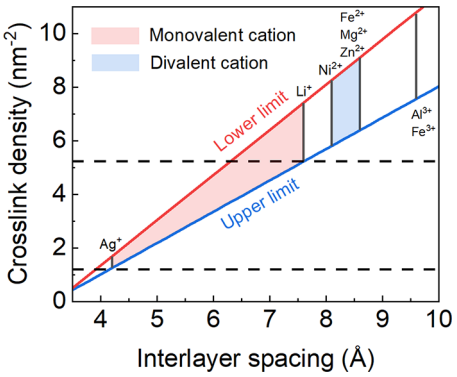

Figure 4. Phase diagram in the plane of cross-link density versus interlayer spacing for the strain engineering of ion-coordinated cellulose nanochannels. The red and blue lines denote the lower and upper limits of channel spacing for different ionic cellulose nanochannels during the shear deformation. The horizontal dashed lines give the smallest cross-link densities in cellulose nanochannels that allow the transport of Ag^+ and Li^+, respectively.

As shown in Figure 4, the locations of different conductive ions are determined by their hydration radius. For a given type of conductive ion, the minimal cross-link density of Ca^{2+} ions in the cellulose nanochannel can be estimated by the location of corresponding ionic hydration radius at the line of the upper limit. In general, monovalent ions are usually used as conductive ions in cellulose nanochannels. Compared to monovalent ions, bivalent and trivalent ions are hard to transport through cellulose nanochannels due to their strong interactions with hydroxyl groups on the CNC (010) surface.[12,13] Monovalent cations with minimal and maximal hydration radii are Ag^+ and Li^+, respectively. For the case of Ag^+ as conductive ions, the minimal cross-link density of Ca^{2+} ions in the cellulose nanochannel should be ~1.2 nm^{-2} before the strain engineering. Similarly, for Li^+, the minimal cross-link density of Ca^{2+} ions in the cellulose nanochannel is 5.23 nm^{-2}.

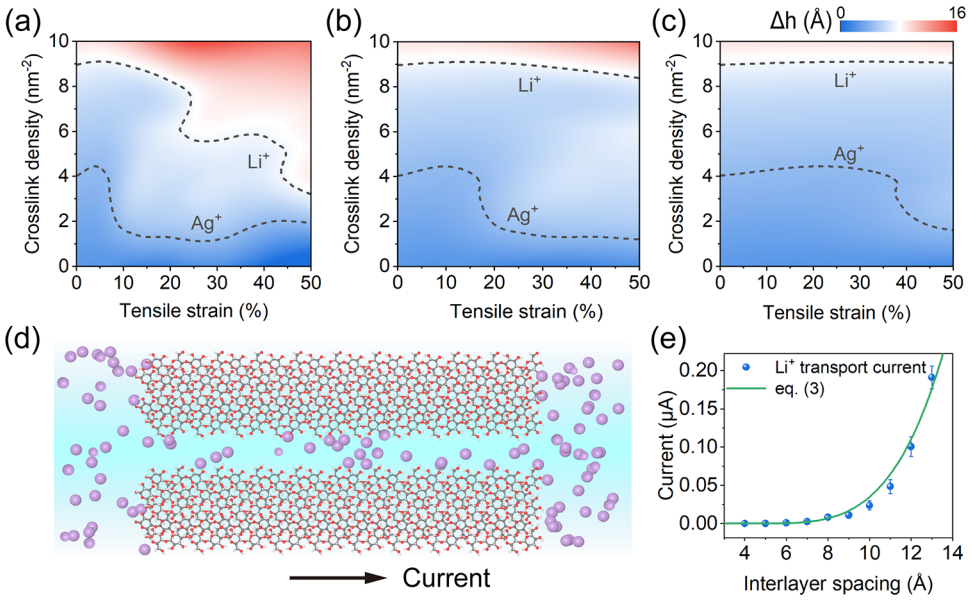

Figure 5. Ionic transport behavior of cellulose nanochannel. (a−c) Representative nephograms of channel spacing in the plane of cross-link density versus tensile strain of RVE with different lengths: (a) 50 nm, (b) 200 nm, and (c) 500 nm, respectively. The dashed curves plot the hydration radius of monovalent ions (Ag^+ and Li^+). (d) Simulation model of Li^+ transport in a cellulose nanochannel driven by an electric field. (e) Current as a function of the channel spacing of cellulose nanochannels for Li^+ transport. The simulated data are fitted by eq 3.

https://doi.org/10.1021/acs.nanolett.4c00867
Nano Lett. 2024, 24, 6262−6268

To further shed light on the strain engineering of Ca^{2+}-intercalated cellulose nanochannels, the size effect of RVE models was considered because the interlayer shear strain distribution is not uniform. In general, there is a competition between the interlayer shear deformation and platelet inelastic deformation.[40,41] Interfacial shear stress in the overlapping zone of the RVE model is transferred from the tension of upper CNCs, which can be understood by the well-known shear-lag model.[38,42,43] The governing equations of the RVE model in Figure 1 can be written as

$$\begin{cases} D\dfrac{\partial^2 u_1(x)}{\partial x^2} - \dfrac{G}{h_c}(u_1(x) - u_2(x)) = 0 \\ D\dfrac{\partial^2 u_2(x)}{\partial x^2} - \dfrac{G}{h_c}(u_2(x) - u_1(x)) = 0 \end{cases} \tag{1}$$

where u_1 and u_2 are the displacement of the top layer and bottom layer, respectively, x is the position coordinates, D is the stiffness of a single layer, G is the shear modulus, and h_c is the distance between two layers. The displacement boundary conditions of the RVE model are given as $u_1(l) = \Delta$ and $u_1'(0) = u_2(0) = u_2'(l) = 0$, where Δ is the right end tensile displacement of the top layer. We thus obtained the DMC as

$$\overline{\delta} = \frac{\varepsilon l}{\varphi(\omega, l)(\varphi(\omega, l) + \coth(\varphi(\omega, l)))} \tag{2}$$

where ω is the cross-link density of intercalated ionic media, ε is the tensile strain, l is the overlapping length of two adjacent CNCs in the RVE model, and $\varphi(\omega, l)$ is a dimensionless parameter, defined as $\varphi(\omega, l) = l\sqrt{G(\omega)/Dh_c(\omega)}$, representing the relative overlapping length. The details of the derivation of $\overline{\delta}$ are shown in the Supporting Information. Based on the obtained $\overline{\delta}$, the interlayer spacing (Δh) of Ca^{2+}-intercalated cellulose nanochannels can be measured from MD simulations.

Figure 5a–c depicts representative nephograms of interlayer spacing in the plane of cross-link density versus the tensile strain of RVE models with overlapping lengths of 50, 200, and 500 nm, respectively. In those nephograms, the contour lines of Ag^+ and Li^+ are plotted to give the boundaries of monovalent ion transport in the Ca^{2+}-intercalated cellulose nanochannels. For RVE models with a small overlapping length, the interlayer spacing of cellulose nanochannels can be effectively regulated by changing the cross-link density of intercalated Ca^{2+} ions and tensile strain. With an increase in overlapping length, the effect of strain engineering on the interlayer spacing is diminished, which is consistent with the relationship between dimensionless DMC and overlapping length (Figure S6). Essentially, when the overlapping length is long, the upper layer trends to change from global slipping to local deformation during the tensile process, while the interlayer spacing is mainly controlled by the cross-link density. The effect of strain engineering is thus limited by the nonuniform interlayer shear,[28,44−46] which has also been reported in other layered 2D materials (e.g., graphene oxide, MoS_2). Therefore, controlling the overlapping length is an effective method to adjust the sensitivity of strain engineering for cellulose-based conductors.

Finally, we show how interlayer spacing affects the current in cellulose nanochannels. In Figure 5d, the model is a cellulose nanochannel filled by water molecules and Li^+ ions. In our simulations, an electric field of 0.05 V/Å was applied along the length direction of the nanochannel, and the interlayer spacing was changed from 4 to 14 Å. Previous studies showed fast ion transport in the cellulose nanochannels by combining with the oxygen atoms in the −OH groups of cellulose and hopping from one to another in a low energy barrier when an electric field is applied.[12,48] For cellulose nanochannels with an interlayer spacing smaller than 2 nm, the ions can hop by combining with oxygen atoms in −OH groups of both sides, which greatly reduces the migration energy barrier. But for cellulose nanochannels whose interlayer spacing is larger than 2 nm, the distance of the −OH groups in both sides is too large for hopping and only −OH groups in one side can be provided for hopping, which leads to a high migration energy barrier. Indeed, a recent study by Li et al. showed that removing the large pores/channels (∼10 μm) by compression can almost double the conductivity of a cellulose-based conductor.[19] Li et al. also showed similar results that pressing a cellulose-based conductor can reduce the channel diameter from 20 to 2 nm and greatly improve the conductivity.[47] This size effect was also demonstrated theoretically by Garg et al. with MD simulations.[48] Therefore, here, we are mainly concerned with the cellulose nanochannels with a width of ∼1 nm for fast ion transport.

The primary data between current and time are shown in Figure S7 and the current after stabilization is summarized in Figure 5e. It shows that the simulated relationship between the current and interlayer spacing can be approximately fitted by the Hagen−Poiseuille equation, which can be expressed as

$$Q = \frac{\pi d^4}{128\mu L}\Delta P \propto d^4 \tag{3}$$

where Q is the volume flow rate, d is the interlayer spacing of nanochannel, μ is the viscosity of the fluid, ΔP is the pressure difference (or voltage difference) between the two ends of the channel, and L is the length of the channel. As shown in Figure 5e, when the interlayer spacing is smaller than 7.0 Å, the simulated current of Li^+ ions is almost zero due to the steric hindrance effect of the cellulose nanochannels. While when the interlayer spacing is larger than 7.0 Å, the simulated current of Li^+ ions increases significantly. Based on the simulation results in Figures 3 and 4, strain engineering can realize the size regulation of cellulose nanochannels with angstrom precision. In recent experiments, the conductivity of a Cu^{2+}-coordinated cellulose conductor can increase as much as several hundred times through expanding the nanochannel width from 3.9 to 8.4 Å. The increase in corresponding current is estimated to be from 2.69×10^{-9} to 0.01 μA. In our MD simulations of Ca^{2+}-intercalated cellulose nanochannels (Figure 3c), strain engineering can change the interlayer spacing from 7.8 to 12 Å when the cross-link density is 9 nm^{-2}, and thus the simulated current can reach a 0.1 μA level. Therefore, strain engineering should be a promising method to regulate interlayer spacing of nanochannels in cellulose-based conductors, realizing fast ion transport and current regulation. We are delighted to note that recent experimental studies have realized the regulation of cellulose nanochannels and achieved satisfactory results of fast ion transport.[12,19] As a new concept of cellulose-based conductors, it can be expected that more efforts in future studies will be devoted to improve the precise control of cellulose nanochannels.

https://doi.org/10.1021/acs.nanolett.4c00867
Nano Lett. 2024, 24, 6262−6268

In summary, based on the calculations of binding energy and bond length, a calcium ion was identified as the optimal ionic cross-link for regulating interlayer spacing of cellulose nanochannels effectively. Our theoretical simulations provide insights into the interlayer spacing limits for the transport of various cations. To clarify the size effect of the RVE, we employed the shear-lag model to explore the regulation of interlayer spacing under tensile strain. We demonstrated that controlling the overlapping length is an effective way to regulate the sensitivity of strain engineering for cellulose-based conductors. Consequently, the transport of Li^+ ions through the cellulose nanochannel was investigated and the application of tensile strain was anticipated to enhance the current of the cellulose-based conductor to the 0.1 μA level.

An effective approach to regulating the interlayer spacing holds the potential to enhance the performance of cellulose-based conductors. Through our multiscale modeling and theoretical analyses, the strain engineering method was proposed to regulate the interlayer spacing precisely. This method should serve as a valuable guide for the design of cellulose-based conductors with superior conductivity and governable current.

■ ASSOCIATED CONTENT

Supporting Information

The Supporting Information is available free of charge at https://pubs.acs.org/doi/10.1021/acs.nanolett.4c00867.

Details of DFT calculations and MD simulations, a mechanical model of strain engineering, formulas to fit the interlayer spacing and cross-link density, the relationship between dimensionless displacement and dimensionless length, primary data of current simulation in cellulose nanochannels, DFT calculations and MD simulations, shear stress−strain curve, competition between cross-links and attraction force of CNCs, the interlayer spacing after tensile, dimensionless displacement, and the current in cellulose nanochannels (PDF)

■ AUTHOR INFORMATION

Corresponding Author

YinBo Zhu − *CAS Key Laboratory of Mechanical Behavior and Design of Materials, Department of Modern Mechanics, University of Science and Technology of China, Hefei 230027, People's Republic of China;* orcid.org/0000-0001-9204-9300; Email: zhuyinbo@ustc.edu.cn

Authors

JiaHao Li − *CAS Key Laboratory of Mechanical Behavior and Design of Materials, Department of Modern Mechanics, University of Science and Technology of China, Hefei 230027, People's Republic of China*

YuanZhen Hou − *CAS Key Laboratory of Mechanical Behavior and Design of Materials, Department of Modern Mechanics, University of Science and Technology of China, Hefei 230027, People's Republic of China*

ZeZhou He − *CAS Key Laboratory of Mechanical Behavior and Design of Materials, Department of Modern Mechanics, University of Science and Technology of China, Hefei 230027, People's Republic of China;* orcid.org/0000-0002-6805-3550

HengAn Wu − *CAS Key Laboratory of Mechanical Behavior and Design of Materials, Department of Modern Mechanics, University of Science and Technology of China, Hefei 230027, People's Republic of China; State Key Laboratory of Nonlinear Mechanics, Institute of Mechanics, Chinese Academy of Science, Beijing 100190, People's Republic of China;* orcid.org/0000-0003-0288-1617

Complete contact information is available at: https://pubs.acs.org/10.1021/acs.nanolett.4c00867

Author Contributions

[§]J.L. and Y.H. contributed equally to this work.

Author Contributions

Y.Z. conceived the idea and designed the research. H.W. supervised the project. J.L., Y.H., and Z.H. performed simulations. J.L. and Y.Z. analyzed data and wrote the paper. All authors commented on the study.

Notes

The authors declare no competing financial interest.

■ ACKNOWLEDGMENTS

This work was jointly supported by the Youth Innovation Promotion Association CAS (2022465), the National Natural Science Foundation of China (12232016, 12172346, and 12202431), and the Natural Science Foundation of Anhui Province (2208085QA24). The numerical calculations have been done on the supercomputing system in Hefei Advanced Computing Center and the Supercomputing Center of University of Science and Technology of China.

■ REFERENCES

(1) Ji, H.; Urban, A.; Kitchaev, D. A.; Kwon, D.-H.; Artrith, N.; Ophus, C.; Huang, W.; Cai, Z.; Shi, T.; Kim, J. C.; Kim, H.; Ceder, G. Hidden Structural and Chemical Order Controls Lithium Transport in Cation-Disordered Oxides for Rechargeable Batteries. *Nat. Commun.* **2019**, *10* (1), 592.

(2) Mrozik, W.; Ali Rajaeifar, M.; Heidrich, O.; Christensen, P. Environmental Impacts, Pollution Sources and Pathways of Spent Lithium-Ion Batteries. *Energy Environ. Sci.* **2021**, *14* (12), 6099−6121.

(3) Yu, J.; Wang, X.; Zhou, M.; Wang, Q. A Redox Targeting-Based Material Recycling Strategy for Spent Lithium Ion Batteries. *Energy Environ. Sci.* **2019**, *12* (9), 2672−2677.

(4) Baars, J.; Domenech, T.; Bleischwitz, R.; Melin, H. E.; Heidrich, O. Circular Economy Strategies for Electric Vehicle Batteries Reduce Reliance on Raw Materials. *Nat. Sustain.* **2021**, *4* (1), 71−79.

(5) Teng, X.; Zhan, C.; Bai, Y.; Ma, L.; Liu, Q.; Wu, C.; Wu, F.; Yang, Y.; Lu, J.; Amine, K. In Situ Analysis of Gas Generation in Lithium-Ion Batteries with Different Carbonate-Based Electrolytes. *ACS Appl. Mater. Interfaces* **2015**, *7* (41), 22751−22755.

(6) Belharouak, I.; Koenig, G. M.; Amine, K. Electrochemistry and Safety of Li4Ti5O12 and Graphite Anodes Paired with LiMn2O4 for Hybrid Electric Vehicle Li-Ion Battery Applications. *J. Power Sources* **2011**, *196* (23), 10344−10350.

(7) Schmuch, R.; Wagner, R.; Hörpel, G.; Placke, T.; Winter, M. Performance and Cost of Materials for Lithium-Based Rechargeable Automotive Batteries. *Nat. Energy.* **2018**, *3* (4), 267−278.

(8) Kang, D. H. P.; Chen, M.; Ogunseitan, O. A. Potential Environmental and Human Health Impacts of Rechargeable Lithium Batteries in Electronic Waste. *Environ. Sci. Technol.* **2013**, *47* (10), 5495−5503.

(9) Hou, Y.; He, Z.; Zhu, Y.; Wu, H. Intrinsic Kink Deformation in Nanocellulose. *Carbohyd. Polym.* **2021**, *273*, No. 118578.

(10) Hou, Y.; Xia, J.; He, Z.; Zhu, Y.; Wu, H. Molecular Levers Enable Anomalously Enhanced Strength and Toughness of Cellulose Nanocrystal at Cryogenic Temperature. *Nano Res.* **2023**, *16* (5), 8036−8041.

(11) Uetsuji, Y.; Hamamoto, R.; Luo, C.; Tsuyuki, Y.; Tsuchiya, K.; Ikura, R.; Takashima, Y. Fiber Morphology Design of Cellulose Composites through Multiscale Simulation. *Int. J. Mech. Sci.* **2023**, *258*, No. 108581.
(12) Yang, C.; Wu, Q.; Xie, W.; Zhang, X.; Brozena, A.; Zheng, J.; Garaga, M. N.; Ko, B. H.; Mao, Y.; He, S.; Gao, Y.; Wang, P.; Tyagi, M.; Jiao, F.; Briber, R.; Albertus, P.; Wang, C.; Greenbaum, S.; Hu, Y.-Y.; Isogai, A.; Winter, M.; Xu, K.; Qi, Y.; Hu, L. Copper-Coordinated Cellulose Ion Conductors for Solid-State Batteries. *Nature* **2021**, *598* (7882), 590−596.
(13) Wu, Z.; Wang, B.; Li, J.; Wu, R.; Jin, M.; Zhao, H.; Chen, S.; Wang, H. Advanced Bacterial Cellulose Ionic Conductors with Gigantic Thermopower for Low-Grade Heat Harvesting. *Nano Lett.* **2022**, *22* (20), 8152−8160.
(14) Salmén, L. Wood Morphology and Properties from Molecular Perspectives. *Ann. For. Sci.* **2015**, *72* (6), 679−684.
(15) Salmen, L.; Olsson, A.-M.; Stevanic, J. S.; Simonovic, J.; Radotic, K. Structural organisation of the wood polymers in the wood fibre structure. *BioRes.* **2011**, *7* (1), 521−532.
(16) Fratzl, P.; Elbaum, R.; Burgert, I. Cellulose Fibrils Direct Plant Organ Movements. *Faraday Discuss.* **2008**, *139*, 275.
(17) Reiterer, A.; Lichtenegger, H.; Tschegg, S.; Fratzl, P. Experimental Evidence for a Mechanical Function of the Cellulose Microfibril Angle in Wood Cell Walls. *Philos. Mag. A* **1999**, *79* (9), 2173−2184.
(18) Chen, B.; Jing, S.; Chen, Q.; Pei, Y.; Deng, T.; Yang, B.; Wang, C.; Li, T. All-Natural, Eco-Friendly Composite Foam for Highly Efficient Atmospheric Water Harvesting. *Nano Energy* **2023**, *110*, No. 108371.
(19) Dong, Q.; Zhang, X.; Qian, J.; He, S.; Mao, Y.; Brozena, A. H.; Zhang, Y.; Pollard, T. P.; Borodin, O. A.; Wang, Y.; Chava, B. S.; Das, S.; Zavalij, P.; Segre, C. U.; Zhu, D.; Xu, L.; Liang, Y.; Yao, Y.; Briber, R. M.; Li, T.; Hu, L. A Cellulose-Derived Supramolecule for Fast Ion Transport. *Sci. Adv.* **2022**, *8* (49), No. eadd2031.
(20) Deng, S.; Sumant, A. V.; Berry, V. Strain Engineering in Two-Dimensional Nanomaterials beyond Graphene. *Nano Today* **2018**, *22*, 14−35.
(21) Gao, E.; Xu, Z. Bio-Inspired Graphene-Derived Membranes with Strain-Controlled Interlayer Spacing. *Nanoscale* **2018**, *10* (18), 8585−8590.
(22) He, Z.; Zhu, Y.; Wu, H. Multiscale Mechanics of Noncovalent Interface in Graphene Oxide Layered Nanocomposites. *Theor. Appl. Mech. Lett.* **2022**, *12* (1), No. 100304.
(23) Peng, Z.; Chen, X.; Fan, Y.; Srolovitz, D. J.; Lei, D. Strain Engineering of 2D Semiconductors and Graphene: From Strain Fields to Band-Structure Tuningand Photonic Applications. *Light: Sci. Appl.* **2020**, *9* (1), 190.
(24) Castellanos-Gomez, A.; Roldán, R.; Cappelluti, E.; Buscema, M.; Guinea, F.; van der Zant, H. S. J.; Steele, G. A. Local Strain Engineering in Atomically Thin MoS2. *Nano Lett.* **2013**, *13* (11), 5361−5366.
(25) John, A. P.; Thenapparambil, A.; Thalakulam, M. Strain-Engineering the Schottky Barrier and Electrical Transport on MoS2. *Nanotechnology* **2020**, *31* (27), No. 275703.
(26) He, X.; Li, H.; Zhu, Z.; Dai, Z.; Yang, Y.; Yang, P.; Zhang, Q.; Li, P.; Schwingenschlogl, U.; Zhang, X. Strain Engineering in Monolayer WS2, MoS2, and the WS2/MoS2 Heterostructure. *Appl. Phys. Lett.* **2016**, *109* (17), No. 173105.
(27) De Sanctis, A.; Mehew, J. D.; Alkhalifa, S.; Withers, F.; Craciun, M. F.; Russo, S. Strain-Engineering of Twist-Angle in Graphene/hBN Superlattice Devices. *Nano Lett.* **2018**, *18* (12), 7919−7926.
(28) He, Z.; Zhu, Y.; Xia, J.; Wu, H. Optimization Design on Simultaneously Strengthening and Toughening Graphene-Based Nacre-like Materials through Noncovalent Interaction. *J. Mech. Phys. Solids* **2019**, *133*, No. 103706.
(29) Zhang, Y.; Gong, S.; Zhang, Q.; Ming, P.; Wan, S.; Peng, J.; Jiang, L.; Cheng, Q. Graphene-Based Artificial Nacre Nanocomposites. *Chem. Soc. Rev.* **2016**, *45* (9), 2378−2395.
(30) Wang, F.; Wang, W.; Mu, X.; Mao, J. Anisotropic Conductive, Tough and Stretchable Heater Based on Nacre-like Crumpled Graphene Composite. *Chem. Eng. J.* **2020**, *395*, No. 125183.
(31) Huang, C.; Peng, J.; Cheng, Y.; Zhao, Q.; Du, Y.; Dou, S.; Tomsia, A. P.; Wagner, H. D.; Jiang, L.; Cheng, Q. Ultratough Nacre-Inspired Epoxy−Graphene Composites with Shape Memory Properties. *J. Mater. Chem. A* **2019**, *7* (6), 2787−2794.
(32) Hou, Y.; Guan, Q.-F.; Xia, J.; Ling, Z.-C.; He, Z.; Han, Z.-M.; Yang, H.-B.; Gu, P.; Zhu, Y.; Yu, S.-H.; Wu, H. Strengthening and Toughening Hierarchical Nanocellulose via Humidity-Mediated Interface. *ACS Nano* **2021**, *15* (1), 1310−1320.
(33) Diederichsen, K. M.; McShane, E. J.; McCloskey, B. D. Promising Routes to a High Li+ Transference Number Electrolyte for Lithium Ion Batteries. *ACS Energy Lett.* **2017**, *2* (11), 2563−2575.
(34) Xue, Z.; He, D.; Xie, X. Poly(Ethylene Oxide)-Based Electrolytes for Lithium-Ion Batteries. *J. Mater. Chem. A* **2015**, *3* (38), 19218−19253.
(35) Wang, R.; Chen, C.; Pang, Z.; Wang, X.; Zhou, Y.; Dong, Q.; Guo, M.; Gao, J.; Ray, U.; Xia, Q.; Lin, Z.; He, S.; Foster, B.; Li, T.; Hu, L. Fabrication of Cellulose−Graphite Foam via Ion Cross-Linking and Ambient-Drying. *Nano Lett.* **2022**, *22* (10), 3931−3938.
(36) Xia, J.; Zhu, Y.; He, Z.; Wang, F.; Wu, H. Superstrong Noncovalent Interface between Melamine and Graphene Oxide. *ACS Appl. Mater. Interfaces* **2019**, *11* (18), 17068−17078.
(37) Gao, E.; Cao, Y.; Liu, Y.; Xu, Z. Optimizing Interfacial Cross-Linking in Graphene-Derived Materials, Which Balances Intralayer and Interlayer Load Transfer. *ACS Appl. Mater. Interfaces* **2017**, *9* (29), 24830−24839.
(38) Liu, Y.; Xu, Z. Multimodal and Self-Healable Interfaces Enable Strong and Tough Graphene-Derived Materials. *J. Mech. Phys. Solids* **2014**, *70*, 30−41.
(39) Tansel, B. Significance of Thermodynamic and Physical Characteristics on Permeation of Ions during Membrane Separation: Hydrated Radius, Hydration Free Energy and Viscous Effects. *Sep. Purif. Technol.* **2012**, *86*, 119−126.
(40) Ni, Y.; Song, Z.; Jiang, H.; Yu, S.-H.; He, L. Optimization Design of Strong and Tough Nacreous Nanocomposites through Tuning Characteristic Lengths. *J. Mech. Phys. Solids* **2015**, *81*, 41−57.
(41) He, Z.; Zhu, Y.; Wu, H. A Universal Mechanical Framework for Noncovalent Interface in Laminated Nanocomposites. *J. Mech. Phys. Solids* **2022**, *158*, No. 104560.
(42) Cox, H. L. The Elasticity and Strength of Paper and Other Fibrous Materials. *Br. J. Appl. Phys.* **1952**, *3* (3), 72−79.
(43) Wei, X.; Naraghi, M.; Espinosa, H. D. Optimal Length Scales Emerging from Shear Load Transfer in Natural Materials: Application to Carbon-Based Nanocomposite Design. *ACS Nano* **2012**, *6* (3), 2333−2344.
(44) He, Z.; Wu, H.; Xia, J.; Hou, Y.; Zhu, Y. How Weak Hydration Interfaces Simultaneously Strengthen and Toughen Nanocellulose Materials. *Extreme Mech. Lett.* **2023**, *58*, No. 101947.
(45) Yu, Z.; Liu, J.; Wei, X. Unraveling Crack Stability and Strain Localization in Staggered Composites by Fracture Analysis on the Shear-Lag Model. *Compos. Sci. Technol.* **2018**, *156*, 262−268.
(46) Xia, W.; Ruiz, L.; Pugno, N. M.; Keten, S. Critical Length Scales and Strain Localization Govern the Mechanical Performance of Multi-Layer Graphene Assemblies. *Nanoscale* **2016**, *8* (12), 6456−6462.
(47) Li, T.; Zhang, X.; Lacey, S. D.; Mi, R.; Zhao, X.; Jiang, F.; Song, J.; Liu, Z.; Chen, G.; Dai, J.; Yao, Y.; Das, S.; Yang, R.; Briber, R. M.; Hu, L. Cellulose Ionic Conductors with High Differential Thermal Voltage for Low-Grade Heat Harvesting. *Nat. Mater.* **2019**, *18* (6), 608−613.
(48) Garg, M.; Zozoulenko, I. Ion Diffusion through Nanocellulose Membranes: Molecular Dynamics Study. *ACS Appl. Bio Mater.* **2021**, *4* (12), 8301−8308.

https://doi.org/10.1021/acs.nanolett.4c00867
Nano Lett. 2024, 24, 6262−6268